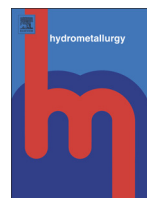




Contents lists available at ScienceDirect

Hydrometallurgy

journal homepage: www.elsevier.com/locate/hydromet

Magnetite precipitation for iron removal from nickel-rich solutions in hydrometallurgy process

Haisheng Han, Wei Sun ^{*}, Yuehua Hu, Xuefeng Cao, Honghu Tang, Runqing Liu, Tong Yue

School of Mineral Processing and Bioengineering, Central South University, Changsha 410083, China

ARTICLE INFO

Article history:

Received 12 June 2015

Accepted 11 January 2016

Available online xxxx

Keywords:

Nickel hydrometallurgy

Potential/pH diagram

Magnetite precipitation

Magnetic flocculation

ABSTRACT

In nickel hydrometallurgical operations, the removal of iron from process liquors was critical, with the method of choice commonly being crystallization (precipitation). In this paper special attention was given to the magnetite precipitate. Potential/pH diagram for Fe–H₂O system was derived at 100 °C, and indicated that the iron ion may precipitate as magnetite at the lower oxidation potential. And the crystallization experiments proved that the iron ion partly precipitate as magnetite by slow oxidation at pH 2.0–2.2 and temperature 90–100 °C. The precipitates could be efficiently separated from the solutions by magnetic flocculation and separation. Further, analyses with Environmental scanning electron microscopy (ESEM) and X-ray Diffraction (XRD) provided a fundamental understanding of the magnetite precipitation process.

© 2016 Elsevier B.V. All rights reserved.

1. Introduction

Since the early 1970s, various hydrolysis–precipitation methods have been developed for iron removal from hydrometallurgical solutions. The widely used techniques, for examples, include the Hematite Process (Ismael and Carvalho, 2003), the Jarosite Process (Swarnkar et al., 1996; Claassen et al., 2002), and the Goethite Process (Davey and Scott, 1976; Pradel et al., 1993). The Goethite Process has the advantages of lower CAPEX over the Hematite Process and producing eco-friendly products relative to the Jarosite Process. The essential feature of the Goethite Process is that the concentration of ferric iron should be maintained at less than 1 g/L during precipitation (Dutrizac, 1987). This requirement can be met by either reducing all ferric ions to the ferrous state (V.M. method) (Bodson, 1972) or by adding the concentrated PLS into a large precipitation vessel at the same rate as goethite precipitation (E.Z. method) (Loan et al., 2006). The E.Z. method led to the development of another two iron removal processes: the Paragoethite Process and Zincor Process (Cubeddu et al., 1996; Meyer et al., 1996). Unlike the Hematite, Jarosite and Goethite Processes, the Paragoethite and Zincor Processes are much less common, in operation at only three commercial zinc processing sites (Wang et al., 2011). Very little information was available on the exact nature of the Paragoethite and Zincor residues, until recent studies of (Loan et al. (2002a)) and Claassen et al. (Loan et al. (2002b)) identified 6-line ferrihydrite and schwertmannite to be the major iron precipitation products.

While the iron removal processes are widely used for solution purification in the zinc industry, their application to nickel sulfate projects has also been explored. Generally, the rejection of iron by

precipitation in the hydrometallurgical processing of nickel follows the same routes used in the zinc industry, and an understanding of these processes therefore comes from the studies centered on the processing of zinc. Research has focused on the removal of iron by goethite precipitation from iron-containing nickel sulfate solutions (Wang et al., 2011; Allan, 1973; Chang et al., 2010). However, in the case of goethite process, the precipitates were “amorphous iron phases”, likely to be nanoscale minerals ferrihydrite or schwertmannite (Loan et al., 2006). The finely grained, poorly crystalline residues generally resulted to the bad filterability (Claassen et al., 2002).

This study conducted goethite process at a lower pH value by V.M method, and found that the iron could partly precipitate in the form of magnetite. The magnetite particles would offset the bad settleability and filterability of the precipitates by magnetic flocculation or magnetic separation. Further Environmental scanning electron microscopy (ESEM) and X-ray Diffraction (XRD) analysis provided a fundamental understanding of the characteristics of the precipitates. And the Eh–pH diagram of iron was plotted for providing persuasive evidence.

2. Experimental

2.1. Materials and preparation

Concentrated acidic NiSO₄/Fe²⁺ feed liquor that contained 0.1 g L^{−1} H₂SO₄ (pH ≈ 1), 107.99 g L^{−1} Ni²⁺ and 6.54 g L^{−1} Fe²⁺ was obtained from the 4th Nickel Smelter of Jinchuan Group Ltd in Gansu province, China. The nickel smelter adopted the pressure oxidative leaching process. As shown in Table 1, the nickel sulfate leaching solution contained a large amount of ferrous ion, as well as a variety of analytes, such as Cd, As, Pb, Cu, Ni, and Mn, accounting for the complication of the nickel-rich solution.

^{*} Corresponding author.

E-mail address: 345340973@qq.com (W. Sun).

Table 1
The properties of nickel sulfate leaching solution.

Analyte	Fe ²⁺	Fe ³⁺	Ni	Cu	Co	S	Na	Pb	Si	As
Content/(g/L)	6.54	0.09	107.99	0.39	1.38	70.23	10.61	0.11	0.060	0.068

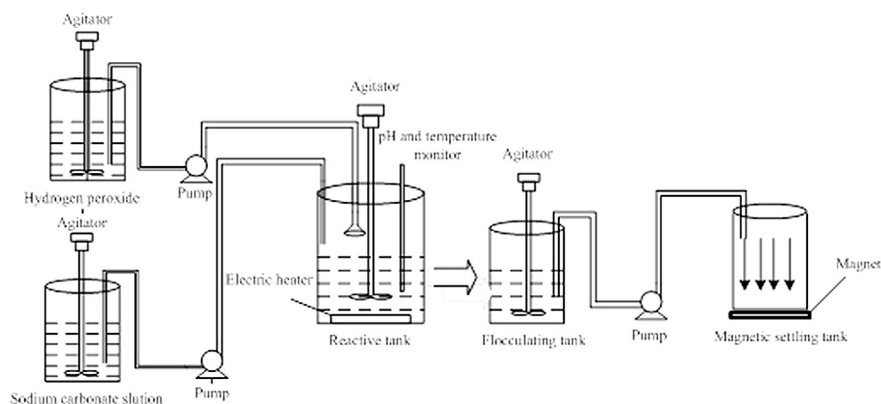


Fig. 1. Diagram of the experimental process, including iron precipitation and removal in the magnetic flocculation process.

2.2. Experimental procedure

The experiments were carried out in a 2 L water-heating reaction kettle by the V.M. process as Fig. 1. The temperature was maintained at 95 °C. The oxidizing agent, hydrogen peroxide, was pumped at a constant rate to keep the low levels of Ferric (<1 g/L) in the reactor. Meanwhile, the neutralizer, sodium carbonate, was pumped at a flow rate designed to control the pH set point (2.0–2.2) and allow the precipitation to proceed. After the precipitation, the polyacrylamide (0.1%) was added to favor the flocculation process and the slurry was pumped to the magnetic settling device for magnetic flocculation and rapid solid–liquid separation. The residues were immediately filtered and the filter cakes were washed with hot sulfuric acid solution (pH 2.0) and dried at 80 °C for 2–3 h. After drying, the samples were divided into several portions for a series of analyses.

2.3. Analytical techniques

Different materials were subjected to chemical analysis and Inductively Coupled Plasma Atomic Emission Spectrometer (ICP-AES)

Table 2
 A_T values at different temperatures.

T/K	298	333	373	423	473	573
A_T	0.511	0.545	0.595	0.689	0.809	1.983

Table 3
The ϕ^0 values of various reactions in Fe–H₂O system at different temperatures.

Reaction no.	Reaction	$\phi^0_{T/V}$	
		25 °C	100 °C
A	$O_2 + 4H^+ + 4e = 2H_2O$	1.228	1.225
B	$2H^+ + 2e = H_2$	0	0.0578
1	$Fe^{2+} + 2e = Fe$	−0.442	−0.373
2	$Fe^{3+} + e = Fe^{2+}$	0.736	0.881
3	$Fe_2O_3 + H_2O + 2e = 2HFeO_2^-$	−1.182	−1.230
4	$Fe_3O_4 + 8H^+ + 8e = 3Fe + 4H_2O$	−0.120	−0.0925
5	$3Fe_2O_3 + 2H^+ + 2e = 2Fe_3O_4 + H_2O$	0.178	0.229
6	$HFeO_2^- + 3H^+ + 2e = Fe + 2H_2O$	0.461	0.530
7	$Fe_3O_4 + 8H^+ + 2e = 3Fe^{2+} + 4H_2O$	0.847	0.750
8	$Fe_3O_4 + 2H_2O + 2e = 2HFeO_2^- + H^+$	−1.862	−1.960
9	$Fe_2O_3 + 6H^+ + 2e = 2Fe^{2+} + 3H_2O$	0.624	0.576

analyses for mass balance purposes, and X-ray Diffraction (XRD) analysis for characterization of the crystalline phase. Qualitative and semi-quantitative data from Environmental Scanning Electron Microscopy (ESEM) analyses were indicative of the phases and genesis of precipitated particles, thus were used to support the XRD, XRF and chemical analysis findings.

2.4. The ϕ -pH diagram of Fe–H₂O system

A brief method for construction of ϕ -pH diagram, which could be constructed from the stoichiometry of reactions and free energy data for the species involved. Either the van't Hoff isotherm or Nernst equation was utilized for the determination of the equilibrium lines of reactions.

The calculation required to obtain the ϕ -pH diagram was based upon the general equilibrium equations for an aqueous system containing ferric and ferrous ions. The basic equation of reactions was shown as formula (1), ϕ_T and pH for this equation could be calculated as formulas (2) and (3):

$$aA_b + nH^+ + ze = bB_a + cH_2O \quad (1)$$

$$\phi_T = \phi_T^0 - 2.303[RTn/(ZF)]pH - 2.303[RTn/(ZF)] \lg(a_{B_a}^b/a_{A_b}^a) \quad (2)$$

$$pH_T = pH_T^0 - 1/n \ln(a_{B_a}^b/a_{A_b}^a). \quad (3)$$

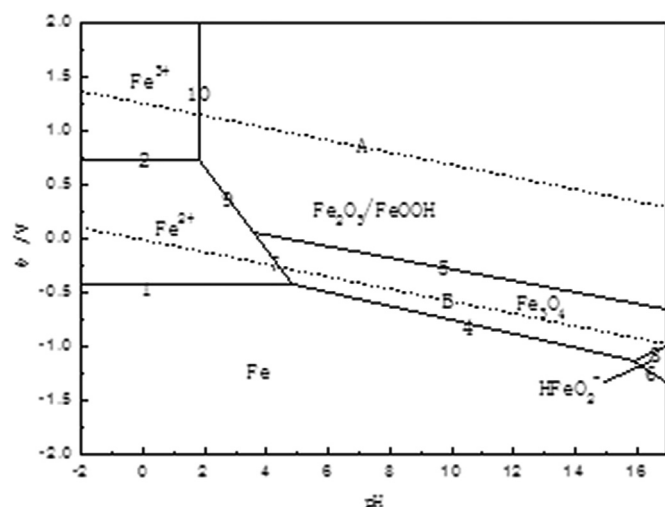
Values of ϕ_T^0 were determined according to Nernst equation, ϕ -pH diagram was obtained based on formulas (2) and (3) sequently, and free energy data of high temperature were required by formula

Table 4
The pH^0 values of various reactions in Fe–H₂O system at different temperatures.

Reaction no.	Reaction	$pH^0_{T/V}$	
		25 °C	100 °C
10	$Fe_2O_3 + 6H^+ = 2Fe^{3+} + 3H_2O$	1.730	1.174

Table 5The activity factors for substances of Fe–H₂O system at different temperatures.

Ion	Ion strength, I/(mol/Kg)	Activity factor, γ_T	
		25 °C	100 °C
Fe ²⁺	0.4	0.2918	0.2163
Fe ³⁺	0.75	0.1917	0.1119
HFeO ₂ [−]	0.1	0.7850	0.7494

**Fig. 2.** Potential/pH diagram for Fe–H₂O system at 100 °C.

(4) (Mu et al., 2011; Zemaitis et al., 2010). Values of A , D , α , β , γ and free energy at 298 K could be required from Post and Robins, (1976); and Lee, (1981).

$$\Delta G_T^\theta = \Delta G_{298}^\theta + \alpha \Delta S_{298}^\theta - \beta + \gamma z$$

$$\alpha = (T-298) \times \left[0.00224 \times \left(T - \frac{T-298}{\ln(T/298)} \right) - 1 \right]$$

$$\beta = \left[T - \frac{T-298}{\ln(T/298)} \right] \times (T-298) \times A$$

$$\gamma = \left[T - \frac{T-298}{\ln(T/298)} \right] \times (T-298) \times D. \quad (4)$$

Average activity coefficients of electrolyte changed with temperature variation. According to (Richardson, (1974), Debye–Hückel

equation, as formula (5), was used to estimate average activity coefficient at high temperature, where γ_{\pm} was average activity coefficient of electrolyte in the solution (calculated by the form of mass concentration), I was ionic strength which could be calculated as formula (6), A_T was a constant which changed with temperature increasing (Table 2), z_+ and z_- were the number of positive and negative ion, respectively.

$$\lg \gamma_{\pm(T)} = \lg \gamma_{\pm(25)} - |z_+ z_-| \frac{\sqrt{I}}{1 + \sqrt{I}} (A_T - A_{25}) \quad (5)$$

$$I = \frac{1}{2} \sum m_i z_i^2 \quad (6)$$

In this work, David's equation was used to calculate the average activity coefficient of electrolyte at 25 °C, shown as formula (7). This equation, with average error of 1.6%, is the widely used method (Robinson and Stokes, 2002).

$$\lg \gamma_{\pm} = -0.50 |z_+ z_-| \left(\frac{\sqrt{I}}{1 + \sqrt{I}} - 0.30 I \right) \quad (7)$$

3. Results and discussion

3.1. The ϕ -pH diagram of Fe–H₂O system

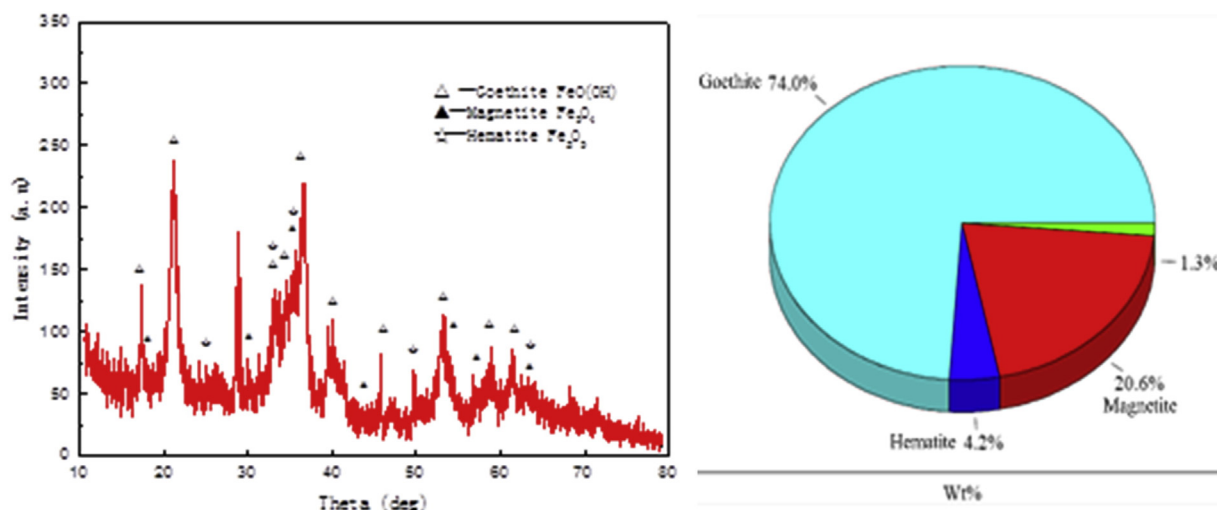
According to the thermodynamic data in Refs. (Zemaitis et al., 2010; Wang-zhong et al., 2010; GU et al., 2011), G_T^θ of substance in Fe–H₂O system could be calculated as formula (3) at 25, and 100 °C, then ΔG_T^θ of different reactions could be obtained according to $\Delta G_T^\theta = \sum G_{T,P}^\theta - \sum G_{T,R}^\theta$. Values of ϕ^θ and pH^θ at different temperatures were listed in Tables 3–4. The activity coefficients of substance in Fe–H₂O system at different temperatures were listed in Table 5.

$$\Delta G^\theta = -ZF\phi^\theta$$

$$pH^\theta = -\frac{\Delta G^\theta}{2.303nRT}$$

Due to the different types of reaction in Fe–H₂O system, the expressions of ϕ and pH were calculated by formula (2) or (3) and then ϕ -pH diagram of Fe–H₂O system (Fig. 2) was realized at ionic mass concentration of 0.1 mol/kg, and temperature 100 °C.

The ϕ -pH diagram of Fe–H₂O system demonstrated that Fe(OH)₃ would form well-defined crystals of FeOOH at temperatures about

**Fig. 3.** XRD patterns of the precipitate.

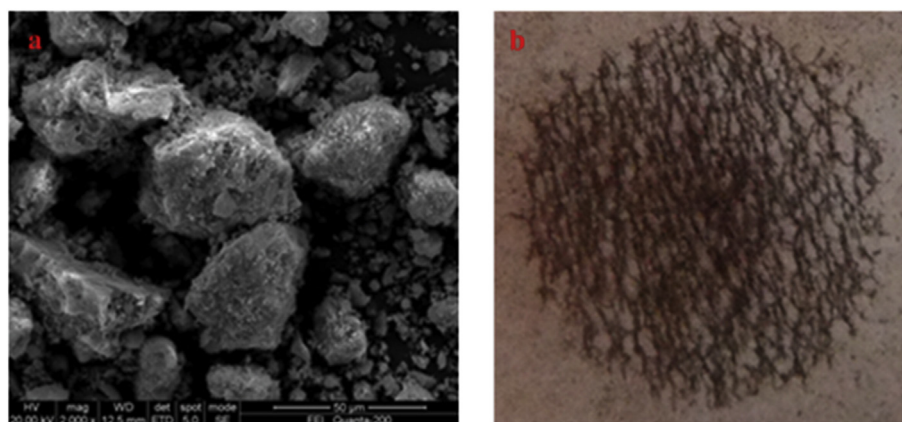


Fig. 4. a. ESEM analysis of iron residues formed during magnetic flocculation process. b. Chain or net structures of magnetic particles under magnetic field. (The picture was taken by a high magnification camera).

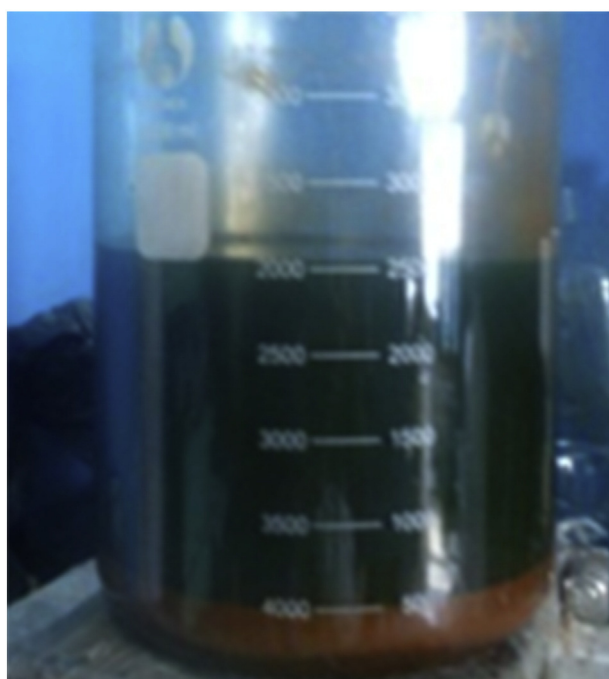


Fig. 5. The settling effect of the precipitates within 2 min in magnetic field.

100 °C, which may decompose to Fe_2O_3 . At the lower oxidation potential (below 0.1 V), the iron may precipitate in the form of Fe_3O_4 , indicating the feasibility of magnetite precipitation from the nickel leaching solutions.

3.2. The iron precipitation and magnetic flocculation

XRD analyses were performed to find out the composition of the precipitates (Fig. 3). Goethite and magnetite were the main phases of the precipitate, and hematite was detected to be minor phase.

Table 6

The results of the iron precipitation and magnetic flocculation.

Samples	Ni	Cu	Fe	Co	S
The leaching solution (g/L)	107.99	0.39	6.63	1.38	
The purified solution (g/L)	101.56	0.31	0.18	1.20	
The washing water (g/L)	10.95	0.033	0.25	0.25	
The washed residue/%	0.59	0.15	48.89	0.033	2.18
The residue after roasting at 600 °C/%	0.71	0.17	59.32	0.08	0.21

In the magnetic field, the magnetic particles aggregated with each other to form chain and net structures (Fig. 4), collecting the fine particles with the help of flocculant during the aggregation. Fig. 5 was the setting effect of the residues within 2 min by magnetic flocculation. The solid–liquid separation was efficient with the residues being compact and the liquid being clear.

Table 6 was the results of the iron precipitation and magnetic flocculation. The iron and nickel concentration of the purified solution were 0.18 g/L and 101.56 g/L respectively, indicating an effective purification with little loss of valuable metals. The iron residue after washing contained 48.89% Fe, and 0.59% Ni, and the iron grade was promoted to 59.32% after dehydration at 600 °C for 0.5 h. The iron residue after dehydration was much more pure, indicating a promising alternative process for the treatment of bulky residues.

3.3. The force analysis and settling velocity of the magnetic particles

Figs. 6 and 7 demonstrated the magnetic field distribution and magnetic field gradient in magnetic settling tank and δ was the perpendicular distance away from the surface of magnet locating the bottom of the settling tank. When δ was 15 cm, the magnetic field intensity was 1.5×10^5 A/m and magnetic field gradient was 2.56×10^5 A/m². The magnetic particles were under the combined action of gravity, magnetic force and hydraulic resistance (Fig.7). The magnetic force could be deduced by the following equation:

$$F_m = \mu_0 K V H \text{grad} H = \mu_0 m \chi H \text{grad} H = 236 \text{mg} = 236 \text{G}$$

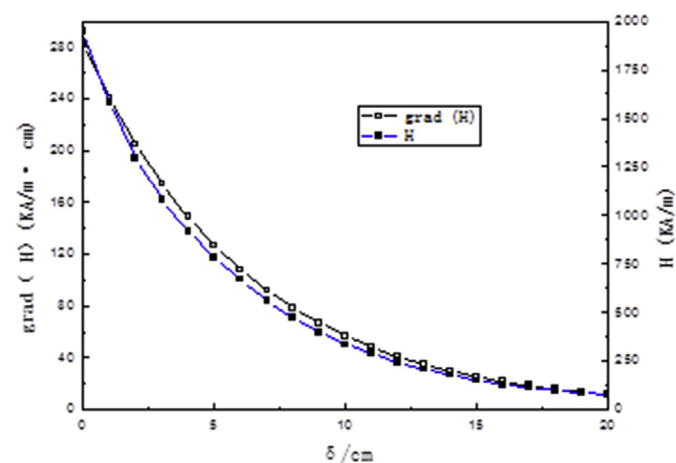


Fig. 6. Magnetic field distribution and magnetic field gradient in the magnetic settling tank.

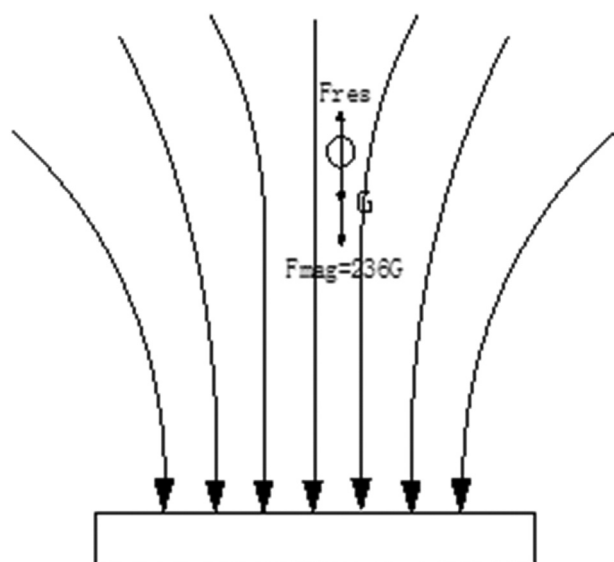


Fig. 7. The force analysis of the particle 15 cm away from the bottom of the settling tank in magnetic field (F_m was magnetic force, G was gravity and F_r was the resistance).

where F_m was the magnetic force, μ_0 was the space permeability $4\pi \times 10^{-7} \text{ N/A}^2$, K was the volume susceptibility, V and m were the volume and the mass of the testing particle respectively, χ was the specific susceptibility and was tested to be $4.8 \times 10^{-3} \text{ m}^3/\text{Kg}$ and G was the gravity of the testing particle. The particle, 15 cm away from the bottom of the settling tank, was subjected to huge magnetic force which was downward and 236 times of the gravity G . The particle would settle to the bottom of the settling tank instantly. The huge magnetic force would contribute to compacting the iron residues.

4. Conclusion

This study proved that the iron ion could be partly precipitated as magnetite by controlling the oxidation potential and pH value. The magnetite particles contributed to the efficient solid–liquid separation by magnetic flocculation and separation. The magnetite precipitation provided a novel method for iron removal from nickel-rich solutions, but it needed to be improved by further studies.

Acknowledgments

This work was supported by autonomous exploration project of graduate student, the 111 Project (No. B14034) and Collaborative

Innovation Center for Clean and Efficient utilization of Strategic Metal Mineral Resources.

References

- Allan, R.W., Method of removing dissolved ferric iron from iron-bearing solutions. 1973, Google Patents.
- Bodson, F.J.J., Recovery of zinc values from zinc plant residue. 1972, Google Patents.
- Chang, Y., et al., 2010. Removal of iron from acidic leach liquor of lateritic nickel ore by goethite precipitate. *Hydrometallurgy* 101 (1), 84–87.
- Claassen, J., et al., 2002. Iron precipitation from zinc-rich solutions: defining the Zincor Process. *Hydrometallurgy* 67 (1), 87–108.
- Cubeddu, F., et al., 1996. The paragoethite process at the ENIRISORSE–Porto Vesme plant. *Iron Control and Disposal*, pp. 147–161.
- Davey, P., Scott, T., 1976. Removal of iron from leach liquors by the “goethite” process. *Hydrometallurgy* 2 (1), 25–33.
- Dutrizac, J., 1987. An overview of iron precipitation in hydrometallurgy. *Canadian Inst Mining Metallurgy Petroleum* 101 6th Ave SW, Ste 320, Calgary Ab T2p 3p4, Canada. CIM BULLETIN.
- GU, Y., et al., 2011. ϵ -pH diagram during pressure leaching of zinc sulfide. *J. Mater. Metall.* 2, 011.
- Ismael, M., Carvalho, J., 2003. Iron recovery from sulphate leach liquors in zinc hydrometallurgy. *Miner. Eng.* 16 (1), 31–39.
- Lee, J., 1981. Elevated temperature potential-pH diagrams for the Cr–H₂O, Ti–H₂O, Mo–H₂O, and Pt–H₂O systems. *Corrosion* 37 (8), 467–481.
- Loan, M., et al., 2002a. Identifying nanoscale ferrihydrite in hydrometallurgical residues. *JOM* 54 (12), 40–43.
- Loan, M., et al., 2002b. Iron oxy-hydroxide crystallization in a hydrometallurgical residue. *J. Cryst. Growth* 235 (1), 482–488.
- Loan, M., et al., 2006. Defining the Paragoethite process for iron removal in zinc hydrometallurgy. *Hydrometallurgy* 81 (2), 104–129.
- Meyer, E., et al., 1996. Iron control and removal at the Zinc Corporation of South Africa. *Iron Control and Disposal*, pp. 163–182.
- Mu, W.-Z., et al., 2011. φ -pH diagram of V–Ti–H₂O system during pressure acid leaching of converter slag containing vanadium and titanium. *Trans. Nonferrous Metals Soc. China* 21 (9), 2078–2086.
- Post, K., Robins, R., 1976. Thermodynamic diagrams for the vanadium–water system at 298 15 K. *Electrochim. Acta* 21 (6), 401–405.
- Pradel, J., et al., 1993. Ferric hydroxide oxide from the goethite process: characterization and potential use. *Ind. Eng. Chem. Res.* 32 (9), 1801–1804.
- Richardson, F.D., 1974. *Physical Chemistry of Melts in Metallurgy*. Academic Press (Elsevier).
- Robinson, R.A., Stokes, R.H., 2002. *Electrolyte Solutions*. Courier Dover Publications.
- Swarnkar, S., Gupta, B., Sekharan, R.D., 1996. Iron control in zinc plant residue leach solution. *Hydrometallurgy* 42 (1), 21–26.
- Wang, K., et al., 2011. The effect of iron precipitation upon nickel losses from synthetic atmospheric nickel laterite leach solutions: statistical analysis and modelling. *Hydrometallurgy* 109 (1), 140–152.
- Wang-zhong, M., et al., 2010. E-pH diagram of ZnS–H₂O system during high pressure leaching of zinc sulfide. *Trans. Nonferrous Metals Soc. China* 20 (10), 2012–2019.
- Zemaitis Jr., J.F., et al., 2010. *Handbook of Aqueous Electrolyte Thermodynamics: Theory & Application*. John Wiley & Sons.